analytical chemistry

pubs.acs.org/ac Article

Proximity Enzymatic Glyco-Remodeling Enables Direct and Highly Efficient Lipid Raft Imaging on Live Cells

Jing Tao, Xiaofei Yu, Yuna Guo, Guyu Wang, Huangxian Ju, and Lin Ding*

Cite This: *Anal. Chem.* 2020, 92, 7232−7239 Read Online

ACCESS | Metrics & More | Article Recommendations | Supporting Information

ABSTRACT: Lipid rafts, highly ordered cell membrane domains mainly composed of cholesterol, sphingolipids, and protein receptors, serve as important functional platforms for regulation of lipid/protein interactions. The major predicament in lipid raft study is the lack of direct and robust visualization tools for in situ tracking raft components. To solve this issue, we herein report a proximity enzymatic glyco-remodeling strategy for direct and highly efficient lipid raft labeling and imaging on live cells. Through cofunctionalization of raft-specific recognition motif and glycan-remodeling enzyme on gold nanoparticles, the fabricated nanoprobe can be specifically guided to the raft domains to perform catalytic remodeling on neighboring glycans. Taking advantage of the abundant glycoconjugates enriched in lipid rafts, this elaborate design achieves the translation of one raft-recognition event to multiple raft-confined labeling operations, thus, significantly increasing the labeling efficiency and imaging sensitivity. The direct covalent labeling also enables in situ and long-term tracking of raft components in live cells. The method possesses broad applicability and potential expansibility, thus, will greatly facilitate the investigations on the complex composition, organization, and dynamics of lipid rafts.

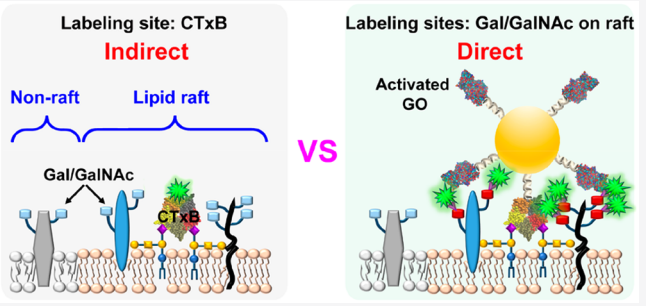

Cellular membranes are laterally heterogeneous.[1] Alongside less organized and more fluid regions, there are distinct, highly ordered membrane domains on cell surface,[2,3] called lipid rafts, which are mainly composed of glycosphingolipids, cholesterol, and selectively recruit certain types of proteins and lipids.[1,4] The typical function of rafts is to segregate specific membrane elements,[1] yielding a microenvironment that can alter the conformation and activities of raft-resident biomolecules,[5−7] regulate protein−protein or protein−lipid interactions, and mediate signaling pathways across the membrane.[8,9] Moreover, the rafts have been considered as the binding sites for many pathogens and bacterial toxins and are preferred by virus budding.[10,11] Rafts also show close relationship with cancer development and progression, which is implicated by the localization of several oncogenic proteins in raft domains.[12−14]

Although the existence of raft domains within cell membrane is well established, the exact nature of rafts and their functional roles in biological processes are still unclear,[1,4] due to the lack of tools for in situ identification and tracking of lipid raft components. Thus, the development of analytical methods for lipid rafts has drawn tremendous attention. Current techniques for studying lipid rafts can be divided into two categories. One is invasive methods, including detergent resistance assay,[15] and mass spectrometry-,[16] Raman spectrometry-[17] or electron microscopy-[18] based label-free methods. These methods usually involve the lysis or fixation of cells, thus fail to directly reflect the native properties of lipid rafts in live cells.[1] The other category is noninvasive fluorescence imaging strategies,[19] where lipid raft-selective probes (such as fluorescent proteins that recognize raft elements, fluorescent lipids that partition into rafts, or fluorescent polysaccharides that interact with raft domains)[20−23] or domain-sensitive probes (including viscosity- and polarity-sensitive dyes)[24,25] are used to differentiate the raft domains. Due to the fast and live-cell observation features, fluorescence imaging is more preferred for probing rafts.

However, there are still several shortcomings for fluorescence methods: (1) They can only illuminate the given binding partners of the recognition probes (strictly speaking, merely the recognition moieties themselves, Figure 1A),[20,21] or the putative lipid raft regions (in the case for fluorescent lipids or environmentally sensitive dyes),[22,24,25] rather than straightforward lighting up the exact components residing in rafts. Thus, they are incompetent for direct visualization and dynamic tracking of raft components. This issue is particularly critical, considering the selective enrichment of a number of

Received: February 23, 2020
Accepted: April 16, 2020
Published: April 16, 2020

https://dx.doi.org/10.1021/acs.analchem.0c00810
Anal. Chem. 2020, 92, 7232−7239

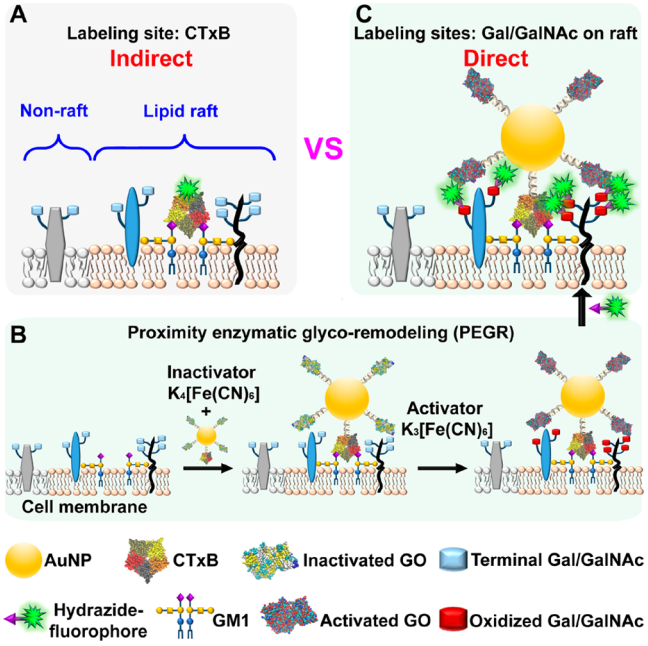

Figure 1. Principle of the proximity enzymatic glyco-remodeling (PEGR) method for lipid raft imaging on live cells. (A) Scheme showing current recognition-based indirect fluorescence methods. (B) Scheme of PEGR. (C) Schematic illustration of the multiple direct labeling of fluorophores on raft components through PEGR.

glycosylated proteins in lipid rafts.[22,26] (2) Because of the rapid intracellular entry of recognition probes or fluorescent lipids,[19,20] just as in the case of cholera toxin B subunit (CTxB),[20] the probes may lose identification capability at an uncertain time point and lead to doubtful results. Thus, although CTxB has been regarded as the gold standard to identify lipid rafts due to its specific binding, as a pentamer, to five monosialotetrahexosylganglioside (GM1) molecules simultaneously,[19−21,27,28] it only allows short-term usage even at low temperature. (3) These probes can only generate one-unit signal from single binding/insertion event (Figure 1A), thus, the imaging sensitivity is largely limited.

To solve the above-mentioned issues, we seek to achieve the direct and highly efficient fluorescence imaging of lipid raft components over extended time scales on live cells. Inspired by the notably high level of protein (lipid) glycosylation on mammalian cell membrane,[29] we propose a proximity enzymatic glyco-remodeling (PEGR) solution by utilizing raft-resident glycans (carbohydrate chains covalently linked to protein or lipids) as the labeling and imaging sites (Figure 1B,C). The idea is implemented through specifically guiding glyco-editing enzyme to the raft domains by raft-recognition motif to perform proximity glycan remodeling. This enables the conversion of one, lipid raft-recognition event to multiple, lipid raft-confined remodeling operations. In this scenario, we fabricate a nanoprobe (GO-AuNP-CTxB) by coimmobilization of CTxB and galactose oxidase (GO) on the surface of gold nanoparticles (AuNPs) using SH-PEG$_7$-COOH as the linker. Owing to the recognition of CTxB toward GM1,[19,20,27,28] the nanoprobe, in GO inactivated state by $K_4[Fe(CN)_6]$,[30,31] can be specifically anchored to the lipid rafts on live cells. Then the GO is activated by $K_3[Fe(CN)_6]$ to perform catalytic oxidation of the hydroxyl group to aldehyde at C-6 position of terminal galactose/*N*-acetylgalactosamine (Gal/GalNAc) of glycan chains only residing in raft regions.[32] This step yields multiple bioorthogonal handles in raft domains for further reaction with fluorescein-5-thiosemicarbazide (FTZ, Figure S1),[33] thus, achieving live-cell lipid raft imaging with substantially enhanced fluorescence sensitivity. The direct, covalent linking of fluorophores to raft components endows the method with a long-term tracking feature, in spite of whether CTxB-mediated probe internalization occurs after probe anchoring. In particular, the obtained glycan-derived signals indicate the expression level of biologically important Gal/GalNAc epitopes in close proximity to the tagged GM1, thus, providing a novel glycan-based research perspective for the complex organization, interactions, and functions of lipid rafts.

EXPERIMENTAL SECTION

Preparation of GO and CTxB Co-Conjugated AuNPs (GO-AuNP-CTxB). The prepared AuNPs of 17.9 nM were diluted by adding equal volume of phosphate buffer (PB) containing 1.82 mg/mL TWEEN 20. After incubation for 30 min at room temperature (r.t.), SH-PEG$_7$-COOH aqueous solution was added with a final concentration of 2 mM. The mixture was allowed to react under a gentle shaking (800 rpm) at 25 °C for 12 h, followed by washing with PB for three times through centrifugation (10000 rpm) at 4 °C for 10 min (15 min for the second and third washing). The precipitate obtained after the third washing (i.e., AuNP-PEG$_7$-COOH) was dispersed in 4-morpholineethanesulfonic acid (MES) buffer, mixed with *N*-(3-(dimethylamino)propyl)-*N*′-ethyl-carbodiimide hydrochloride (EDC, 1.2 mM) and *N*-hydroxysulfosuccinimide sodium salt (sulfo-NHS, 6 mM), and allowed to react under shaking (800 rpm) at 25 °C for 2 h. After washing with PB for three times by centrifugation (10000 rpm) at 4 °C, the final precipitate was dispersed in borate buffer with a concentration of 17.9 nM. Then to 82.3 μL of EDC-activated AuNP-PEG$_7$-COOH solution, 2.7 μL of 3.7 mg/mL GO and 15.1 μL of 56 μg/mL CTxB (the molar ratio of GO to CTxB, i.e. G:C ratio, is 12.0:1.0) were added and allowed to react under shaking (800 rpm) at 25 °C for 4 h. After washing, respectively, with Tris-HCl containing 3% bovine serum albumin (BSA), PB containing 0.05% TWEEN 20, and PB by centrifugation (10000 rpm) at 4 °C, the final probe, GO-AuNP-CTxB, was dispersed in PB and stored in the dark at 4 °C. The counterpart probes with different protein constitution or different protein molar ratios were prepared by the same procedures.

PEGR-Based Lipid Raft Imaging on Live Cells. MCF-7 (or MDA-MB-231, A549) cells were seeded in four-well confocal dishes and cultured in a 37 °C incubator for 24 h. After discarding the culture medium, the cells were blocked in 140 μL of phosphate-buffered saline (PBS) containing 1% BSA and 10% goat serum at 37 °C for 1 h. Then the cells were washed three times with PBS and placed in an ice−water bath for 10 min, followed by adding 100 μL GO-AuNP-CTxB (or other counterpart probes) solution containing 50 mM $K_4[Fe(CN)_6]$. After incubation at 4 °C for 30 min, the cells were washed gently for three times with PBS, and incubated in 100 μL of PBS containing 30 mg/mL D-(+)-galactose (D-Gal) and 50 mM $K_4[Fe(CN)_6]$ in an ice−water bath for 40 min. Then the cells were washed with PBS gently for three times, and allowed to react with 100 μL of PBS containing 10 mM $K_3[Fe(CN)_6]$ at 4 °C for 30 min. After washing with PBS for three times, the cells were subjected to reaction with 100 μL of PBS containing 10 mM aniline, 100 μM FTZ, and 5% fetal bovine serum (FBS) at 4 °C for 1 h, followed by washing for

https://dx.doi.org/10.1021/acs.analchem.0c00810
Anal. Chem. 2020, 92, 7232−7239

three times with PBS. The cells were then imaged with SP8 confocal laser scanning microscopy (CLSM) at stationary parameters including the laser intensity, exposure time, and objective lens. All images were digitized and analyzed by Leica Application Suite Advanced Fluorescence (LAS AF) software.

To demonstrate the dependence of PEGR on GO activation, a control experiment was also performed by omitting the $K_3[Fe(CN)_6]$ reactivation step with other operation unchanged.

To verify the enhancement of imaging sensitivity by PEGR-based method, MCF-7, MDA-MB-231, and A549 cells were separately subjected to seeding, blocking, and PEGR, followed by a reaction with 100 μL of PBS containing 10 mM aniline, 100 μM hydrazide-AF647, and 5% FBS at 4 °C for 1 h. After washing for three times with PBS, the cells were finally imaged with CLSM.

Demonstration of Lipid Raft Imaging Specificity by 7-Ketocholesterol (7KC) Treatment. To prepare 7KC stock solution (3.74 mM), after heating 90 μL of methyl-β-cyclodextrin (mβCD, 50 mg/mL) aqueous solution to 80 °C in a water bath, 2.5 μL of 15 mg/mL 7KC ethanol solution was added every 5 min under stirring with a total addition amount of 10 μL. The mixture was kept under stirring until it became clear, followed by storage at −20 °C until use. The 7KC-based, raft-destroying assay was performed in two ways: (1) pretreating MCF-7 cells with 7KC before PEGR and (2) treating cells with 7KC after FTZ reaction. For the first one, after cell seeding and blocking, the cells were incubated in PBS containing 120 μM 7KC at 37 °C for 30 min. After washing with PBS for three times and incubation in an ice−water bath for 10 min, the cells were subjected to PEGR, FTZ reaction and imaging procedures, as mentioned in PEGR-Based Lipid Raft Imaging on Live Cells. For the second one, the cells after PEGR and FTZ reaction were allowed to incubate with 120 μM 7KC solution at 37 °C for 30 min, followed by three-time washing and CLSM imaging.

Long-Term Tracking of Lipid Raft Components in Live Cells. Group 1: after seeding and blocking, the MCF-7 cells were subjected to PEGR. After washing gently with PBS for three times, the cells were allowed to react with 100 μL of PBS containing 10 mM aniline, 100 μM hydrazide-AF647, and 5% FBS at 4 °C for 1 h. Group 2: the blocked MCF-7 cells were allowed to incubate with 10 μg/mL CTxB-AF647 in an ice−water bath for 30 min. After washing for three times with PBS, the cells from the two groups were incubated with RPMI-1640 complete medium at 37 °C for different periods of time and finally imaged with CLSM.

RESULTS AND DISCUSSION

Preparation and Characterization of CTxB-AuNP-GO. Our initial motivation was to directly label raft components with fluorescence reporters rather than relying on the reporter linked to the recognition or insertion motifs. To achieve this, we turned to the numerous glycoproteins and glycolipids in raft domains, and utilized their sweet decoration as the labeling sites. Owing to the abundance in the glycan chains,[34] Gal/GalNAc was chosen as the remodeling target, and correspondingly, GO, a highly efficient Gal oxidase,[30,31] was chosen as the glyco-remodeling enzyme. To confine the remodeling events in lipid rafts, CTxB was utilized for anchoring GO to rafts.[19,20,27,28] Thus, our work started from the harnessing of these two functional proteins by using AuNPs as the coimmobilization platform due to their unique characteristics, such as excellent biocompatibility, large surface-to-volume ratio, facile functionalization, and so on.[35] The AuNPs, prepared by a classical citrate-reduction method,[36] showed a diameter of 20 nm, as reflected by transmission electron microscopy (TEM) image (Figure 2A), a hydrodynamic

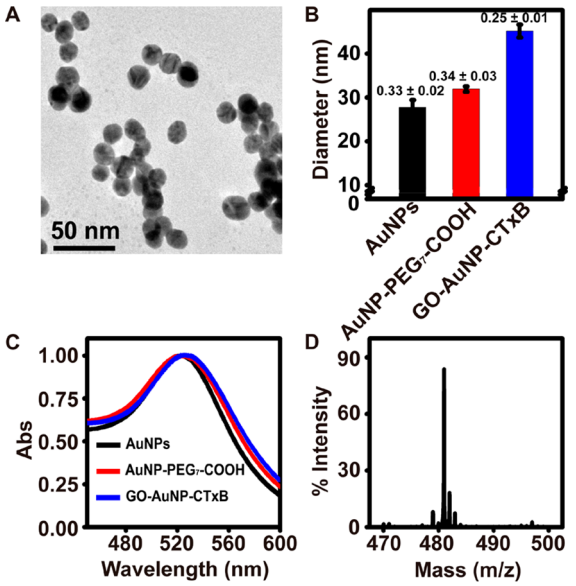

Figure 2. Characterization of the probe synthesis. (A) TEM image of AuNPs. (B) Hydrodynamic diameter and (C) UV−vis spectra of AuNPs, AuNP-PEG$_7$-COOH, and GO-AuNP-CTxB. The values labeled above the columns in (B) are the corresponding PDI. (D) MALDI-TOF MS of AuNP-PEG$_7$-COOH.

diameter of 28 nm with a polydispersity index (PDI) of 0.33, as measured by dynamic light scattering (Figure 2B), and a characteristic UV−vis absorption peak at 521.5 nm (Figure 2C).[37] To increase the stability of AuNPs and endow flexibility to the linked proteins, the as-prepared AuNPs were modified by SH-PEG$_7$-COOH as a linker to yield AuNP-PEG$_7$-COOH. The mass spectrometry (MS) peak with m/z of 481 confirmed successful conjugation of SH-PEG$_7$-COOH (Figure 2D). Then GO and CTxB with a molar ratio of 12.0:1.0 (vide infra) were cocoupled to AuNP-PEG$_7$-COOH under EDC/sulfo-NHS conditions. This step led to an increase in diameter of the AuNP probe from 32 to 45 nm (Figure 2B) and a red shift of the absorption peak from 523.0 to 525.5 nm (Figure 2C), suggesting the successful preparation of the final probe GO-AuNP-CTxB.[38] The PDI of 0.25 for GO-AuNP-CTxB (Figure 2B) indicated a moderate size distribution and homogeneity. The amount of GO assembled on AuNPs was estimated to be 9 through respective determination of the GO and AuNP concentration using a Gal/GO Assay Kit and inductively coupled plasma-mass spectrometry (ICP-MS).

Lipid Raft-Targeted Glyco-Remodeling for Lipid Raft Imaging on Live Cells. With the probe synthesized, the feasibility of performing PEGR for lipid raft imaging on live cells was evaluated using MCF-7 as the model cell type. The key for achieving spatial control of remodeling on live adhered cells is the stringent separation of anchoring and remodeling events,[32] that is, the GO should be inactivated during the recognition process. To this end, $K_4[Fe(CN)_6]$ (Fe^{II}) was used to inhibit GO activity, and after binding and washing, $K_3[Fe(CN)_6]$ (Fe^{III}) was used to activate GO to oxidize the terminal Gal/GalNAc in close proximity to the probe.[30,31] The

https://dx.doi.org/10.1021/acs.analchem.0c00810
Anal. Chem. 2020, 92, 7232−7239

oxidization transforms the hydroxyl group at C-6 to aldehyde, which can efficiently react with fluorophore-labeled hydrazide, such as FTZ, hydrazide-AF647, and so on.[33] To demonstrate PEGR, a control probe, GO-AuNP, with only GO immobilized on the surface of AuNPs via SH-PEG$_7$-COOH was also prepared. Then we performed the following experiments using each type of probes: (1) incubation of MCF-7 cells with the Fe^{II}-inhibited probes of 17.9 nM for 30 min (vide infra), (2) extensive washing, (3) with or without reactivation by $K_3[Fe(CN)_6]$, and (4) reaction with FTZ and imaging by CLSM. For GO-AuNP-CTxB, in the presence of $K_3[Fe(CN)_6]$ reactivation, noticeable fluorescent signal could be observed at the cell periphery, indicating the existence of lipid raft domains on cell surface, whereas without $K_3[Fe(CN)_6]$ reactivation, indiscernible fluorescence could be obtained, suggesting the dependence of fluorescence generation on GO remodeling (Figure 3A). However, for GO-AuNP, in spite of whether

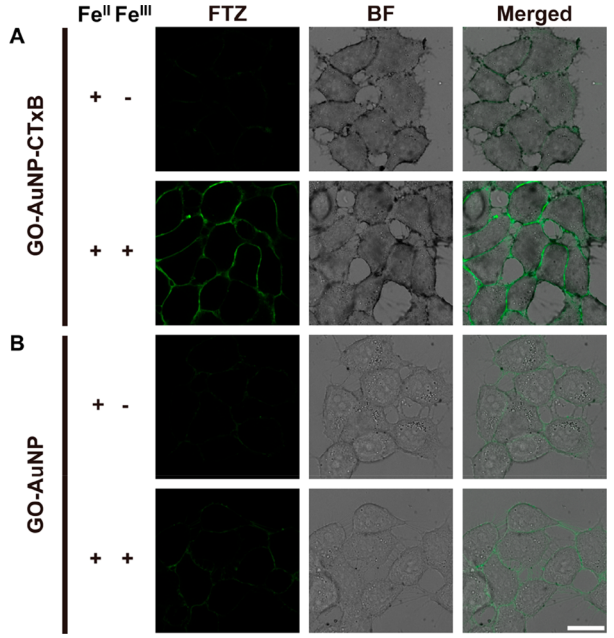

Figure 3. Demonstration of the feasibility of PEGR-based lipid raft imaging on live cells. CLSM images of MCF-7 cells after (1) incubation with GO-AuNP-CTxB or GO-AuNP followed by washing, (2) no treatment or treatment with $K_3[Fe(CN)_6]$, and (3) FTZ reaction. Ex: 488 nm; Imaging window: 505−565 nm. Scale bar: 20 μm.

reactivation was performed, negligible signal could be observed (Figure 3B), suggesting the indispensable role of CTxB for cell surface anchoring. Compared with Figure 3B, the dark-contrasted objects at the cell periphery in bright field (BF) images in Figure 3A, corresponding to the bound GO-AuNP-CTxB on cell surface, also provided proof of CTxB-mediated probe anchoring. The absence of FTZ fluorescence in the case of GO-AuNP with $K_3[Fe(CN)_6]$ reactivation excluded the possibility of nonspecific adsorption of cell membrane toward GO and AuNPs (Figure 3B, bottom). In addition, the indiscernible fluorescence in the top rows of Figure 3A and B suggested the successful inhibition of GO by $K_4[Fe(CN)_6]$ of 50 mM. From these three rows' data, FTZ adsorption could be excluded (Figure 3). The cells undergoing GO-AuNP-CTxB (or AuNP-PEG$_7$-COOH, GO-AuNP) incubation in the presence of $K_4[Fe(CN)_6]$, $K_3[Fe(CN)_6]$ reactivation, and 5 h incubation displayed a cell viability higher than 80% (Figure S2), as examined by CCK8 assay, suggesting acceptable cytocompatibility of the proposed method.

Optimization of Probe Composition and Recognition Conditions. For GO-AuNP-CTxB, it can be reasonably speculated that if the proportion of CTxB is too high, although it is beneficial to lipid raft recognition, the remodeling efficiency is compromised; on the contrary, if the proportion of GO is too high, there will be insufficient recognition motif for guiding probe binding. To optimize the proportion of the two proteins, we fixed the total protein concentration as 1.6 μM for coupling to AuNP-PEG$_7$-COOH (17.9 nM), and adjusted the relative molar ratio of GO to CTxB (i.e., G:C ratio). For each recipe, PEGR, FTZ reaction and CLSM imaging were sequentially performed. As expected, along with decreasing G:C ratio, the FTZ fluorescence intensity (FI) first raised to a plateau and then decreased (Figure 4A,D). The

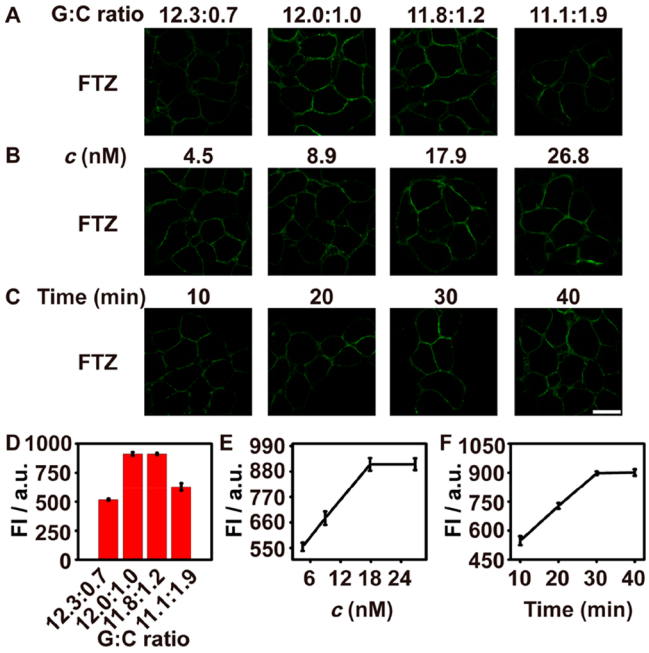

Figure 4. Optimization of probe composition and recognition conditions. (A) CLSM images of MCF-7 cells after PEGR and FTZ reaction using GO-AuNP-CTxB probes prepared with different ratios of GO to CTxB (G:C ratio). (B) CLSM images of MCF-7 cells after incubation with Fe^{II}-inactivated GO-AuNP-CTxB (G:C ratio is 12.0:1.0) of different concentrations for 30 min followed by reactivation and FTZ reaction. (C) CLSM images of MCF-7 cells after incubation with Fe^{II}-inactivated GO-AuNP-CTxB (G:C ratio is 12.0:1.0) of 17.9 nM for different periods of time followed by reactivation and FTZ reaction. Scale bar: 20 μm. (D−F) The average FI at the cell periphery from (A) to (C), respectively. Data are represented as average ± standard deviation (from three independent measurements, counting 30 cells each time).

optimum ratio, 12.0:1.0, was identified when maximum FI was obtained. With probe composition determined, the concentration and recognition time of the probe were then optimized. The variation of probe concentration identified an ideal value of 17.9 nM (Figure 4B,E). With respect to the recognition time, the FI from FTZ followed an initial increase and then plateau dependence pattern, with an inflection point at 30 min (Figure 4C,F).

https://dx.doi.org/10.1021/acs.analchem.0c00810
Anal. Chem. 2020, 92, 7232−7239

Demonstration of the Lipid Raft Imaging Specificity. To confirm that the observed fluorescence signals were indeed from lipid rafts, three groups of experiments were performed (Figure 5). Due to the tight accumulation of molecules in lipid

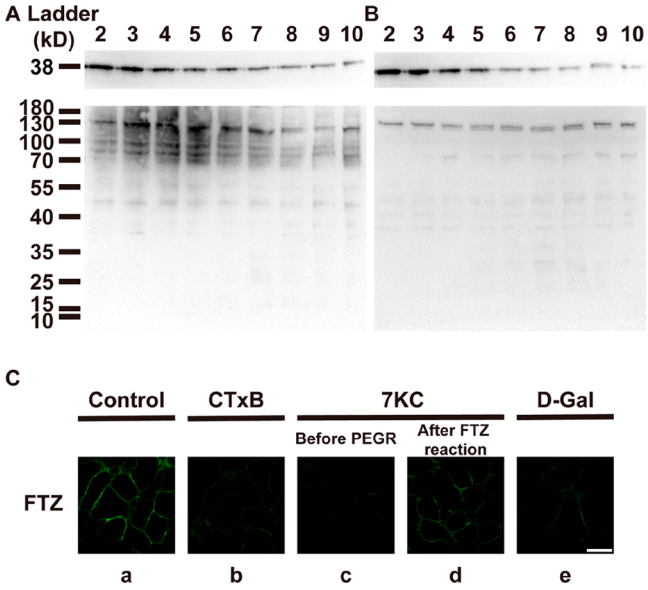

Figure 5. Demonstration of imaging specificity. Western blots of OptiPrep gradient-fractionated lysates from (A) MCF-7 cells after PEGR and biotin hydrazide reaction and (B) untreated MCF-7 cells using antibodies to annexin II (top) and biotin (bottom). (C) CLSM image of (a, control) MCF-7 cells after PEGR and FTZ reaction, and CLSM images of MCF-7 cells after PEGR and FTZ reaction (b) with extra CTxB added at the probe incubation step, (c) with 7KC added before the probe incubation step, (d) with 7KC added after FTZ reaction step, or (e) with D-Gal added at the $K_3[Fe(CN)_6]$ reactivation step. Scale bar: 20 μm.

rafts, they are insoluble in detergents, thus, extraction of detergent-resistant membrane (DRM) by density gradient centrifugation followed by Western blot (WB) is a typical method for probing raft composition.[26,39,40] Thus, we utilized this method to evaluate the raft domain-specificity of our strategy by labeling PEGR-treated cells with biotin hydrazide. In order to eliminate the influence of AuNPs on the distribution of raft components in density fractions, dithiothreitol (DTT) was added after biotin hydrazide labeling to release AuNPs from cell surface. Then the cell lysates were collected, fractioned by centrifugation in a discontinuous OptiPrep gradient, and analyzed by WB with an antibiotin antibody.[39] Annexin II, a lipid raft marker protein,[12,41] was also blotted to indicate the raft-enriched fractions. As shown in Figure 5A, the bands at 38 kDa, corresponding to annexin II, displayed greater signal in lower-density fractions, thus, indicating these more buoyant fractions were rich in raft components. Consistent with this, a significant amount of biotin-labeled proteins could be observed in these lower-density fractions rather than in higher-density ones for the treated cells (Figure 5A), whereas there was only a background-leveled biotin signal evenly distributed in fractions for untreated control cells (Figure 5B). These results suggest that the GO-AuNP-CTxB based PEGR mainly occurs in raft domains. It should be noted that AuNPs of smaller size are beneficial for better raft labeling resolution. In our case, the contribution from nonraft labeling could be largely ignored considering that the diameter of the final GO-AuNP-CTxB probe was 45 nm, a value considerably smaller than the 200 nm commonly recognized as the size for raft domains.[2]

To demonstrate the recognition role of CTxB in the probe, a CTxB competition assay[20] was performed by adding an excessive amount of CTxB (10 μg/mL) together with Fe^{II}-inhibited GO-AuNP-CTxB in the probe anchoring step. The FTZ fluorescence was substantially decreased due to the reduced binding of GO-AuNP-CTxB in the presence of excess CTxB (Figure 5C, b), demonstrating that PEGR was dependent on CTxB recognition.

To further verify the lipid raft-confined labeling, we utilized a lipid raft-destroying agent, 7KC,[42] to break the raft domains before performing PEGR. 7KC can replace cell membrane cholesterol, leading to the conversion from ordered state to disordered state (nonraft domain).[42] The pretreatment by 7KC with an optimal concentration of 120 μM (Figure S3) for 30 min before PEGR led to virtually no FTZ signal observed on cell surface (Figure 5C, c), which could be attributed to the failure of GO-AuNP-CTxB binding to destroyed raft domains. However, when the 7KC treatment was performed after PEGR and FTZ reaction, an obvious fluorescence could be observed on cell periphery (Figure 5C, d). The FI was 79% of that of cells without 7KC treatment (Figure 5C, a). This phenomenon is very interesting. First, it is consistent with the above-mentioned results. Since PEGR is accomplished before 7KC addition, most of the already-labeled glycoconjugates may remain on cell surface after 7KC treatment. Second, this result also suggests a unique feature of our proposed strategy that it not only lights up the lipid rafts on live cells, but also directly attaches a robust label on the raft glycoconjugates, thus, enabling long-term tracking of these raft components, even though they enter the cells.

The glycan remodeling specificity of GO toward Gal/GalNAc was also examined by adding an excessive amount of D-Gal together with $K_3[Fe(CN)_6]$ during reactivation step.[33] As expected, an obvious decrease of FTZ fluorescence was observed (Figure 5C, e), due to the inhibition of GO activity by a mass of D-Gal surrounding GO. Taken together, these results demonstrate that our method indeed performs Gal/GalNAc remodeling only in raft domains.

Demonstration of the High Raft-Labeling Efficiency. The involvement of GO-mediated glyco-remodeling endows the method with a high raft-labeling efficiency. To demonstrate this, CTxB-AF647 was used as the model probe[27] that reporter fluorophore was directly linked to CTxB, and the concentration of CTxB-AF647 was optimized to be 10 μg/mL when maximum AF647 fluorescence was observed (Figure S4). To exclude the influence from fluorescence efficiency on imaging performance, hydrazide-AF647 was utilized to replace FTZ for reaction with aldehyde. Then we implemented lipid raft imaging via each method: (1) PEGR followed by hydrazide-AF647 reaction and (2) CTxB-AF647 binding, under the respective optimal conditions on three types of cell lines, MCF-7, MDA-MB-231 and A549. Compared with CTxB-AF647 labeling method, substantially brighter AF647 fluorescence could be observed for PEGR-based method on all cell types (Figure 6A), demonstrating the highly efficient labeling and imaging capabilities of our method. The corresponding FI was also recorded, and an approximately 2-fold signal enhancement was obtained by our method compared with the CTxB-AF647 based method (Figure 6B,C). This could be attributed to (1) abundant Gal/GalNAc-bearing glycoconju-

https://dx.doi.org/10.1021/acs.analchem.0c00810
Anal. Chem. 2020, 92, 7232−7239

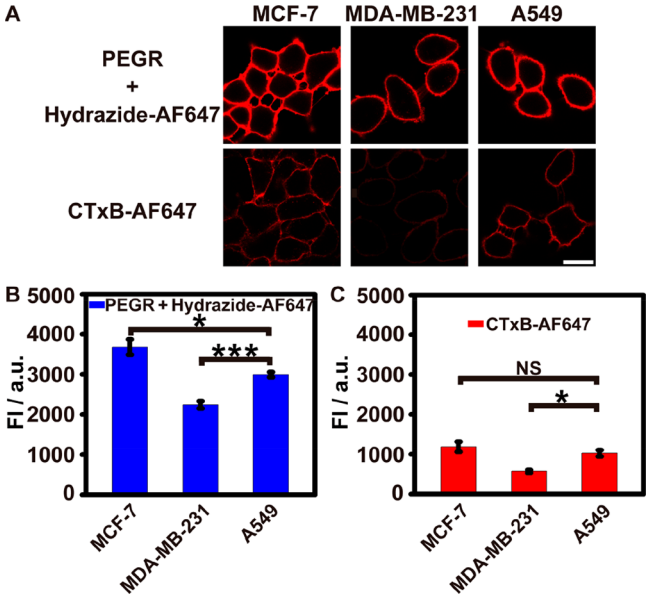

Figure 6. Demonstration of the enhancement of imaging sensitivity by the PEGR-based method. (A) CLSM images of MCF-7, MDA-MB-231 and A549 cells after PEGR and hydrazide-AF647 reaction (top) or CTxB-AF647 labeling (bottom). (B, C) The average FI at the cell periphery from (A). Data are represented as average ± standard deviation (from three independent measurements, counting 30 cells each time). Ex: 647 nm; Imaging window: 657−700 nm. Scale bar: 20 μm. Statistical analysis: Student's *t*-test ($0.01 < {}^{*}p < 0.05$; ${}^{***}p < 0.001$; NS, not significant).

gates surrounding GM1 as labeling sites and (2) recycling usage of GO (walking on the rafts) and multiple assembled GO on AuNPs. The contribution from GO was further evidenced by a noticeable decrease of FTZ signal along with replacing more GO with BSA of equimolar quantities in the GO (BSA)-AuNP-CTxB counterpart probes (Figure S5). Taken together, our method achieves the transformation of one lipid raft recognition event to multiple labeling operations, that is, 1:*n* recognition to labeling ratio.

Among the three cell types examined, MCF-7 and A549 cells displayed strong signals, while MDA-MB-231 cells showed the lowest (Figure 6A). By virtue of the improvement of imaging sensitivity, the PEGR-based imaging revealed statistically significant difference of FI between MCF-7 and A549 cells (Figure 6B), whereas using CTxB-AF647, these two types of cells displayed similar FI (Figure 6C). These data demonstrate the wide applicability of the proposed method and also suggest that our method provides an unprecedented opportunity to reveal the subtle difference of lipid raft coverage on live cells.

Long-Term Tracking of Lipid Raft Components in Live Cells. Besides contributing to enhancement of imaging sensitivity, the proposed method also enables in situ and long-term tracking of lipid raft-associated components (Figure 7), which is a difficult-to-achieve goal for current raft-studying fluorescence tools. This is because these methods fail to directly leave a label on the exact lipid raft components. The issue will affect the raft-identification accuracy when the probe quickly leaves the raft domains. The rapid intracellular entry of CTxB[20] was shown by incubating CTxB-AF647 with live cells. After incubation for 30 min, obvious AF647 signals could be observed inside MCF-7 cells, and along with time extension, the fluorescence at the cell periphery became dim and then totally disappeared (Figure 7B). The translocation of

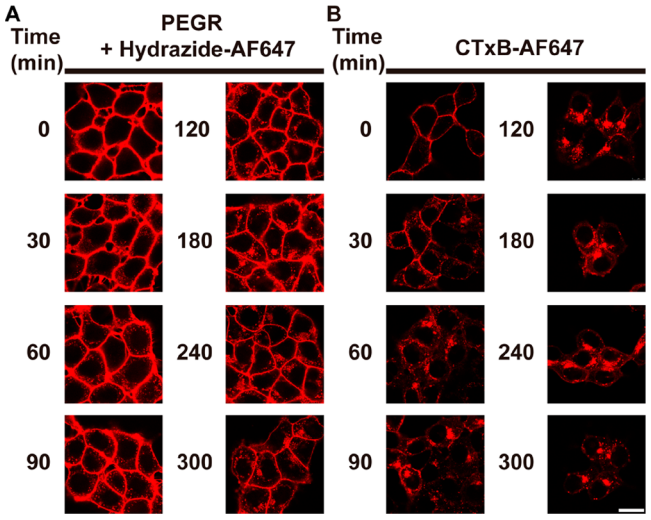

Figure 7. Long-term tracking of lipid raft components in live cells. (A) CLSM images of MCF-7 cells after PEGR, hydrazide-AF647 reaction and subsequent incubation for different periods of time. (B) CLSM images of MCF-7 cells after CTxB-AF647 labeling and subsequent incubation for different periods of time. Scale bar: 20 μm.

fluorescence reflected the internalization process of CTxB. In the contrary, the proposed method yielded covalent labels on the glycosylated lipid raft components, leading to the observation of an unambiguous AF647 fluorescence at cell boundary even after incubation for 300 min (Figure 7A). The gradually increased fluorescence inside cells could be attributed to the endocytosis of the labeled raft components, which is a common phenomenon for raft molecules to execute functions, such as mediation of ligands to enter cells, triggering of signaling events,[43] or regulation of raft composition and distribution.[44] Thus, this observation not only provides evidence for the dynamic nature of raft domains, but also highlights the potential of utilizing the PEGR strategy for tracing the endocytosis and subcellular localization of raft components, in particular, glycoconjugates for a long time frame.

CONCLUSION

In conclusion, a proximity enzymatic glyco-remodeling strategy has been developed for direct and highly efficient lipid raft labeling and imaging on live cells. The method integrates the lipid raft-recognition capability of CTxB and Gal/GalNAc-catalytic oxidation capability of GO on AuNPs, enabling the translation of one lipid raft recognition event to multiple lipid raft-confined glyco-remodeling operations. The straightforward and highly efficient raft labeling leads to an enhancement of raft imaging sensitivity and allows in situ and long-term tracking of raft components. This is a novel perspective for lipid raft imaging. The proposed method can be easily adapted with the addition of more specific raft-recognition molecules to the repertoire. When combined with other techniques such as MS,[45] the method may be further exploited for colocalization analysis of glycoproteins/glycolipids surrounding GM1 and also profiling of raftophilic elements. Thus, the proposed method provides an elegant tool for probing raft organization and composition and will facilitate the revelation of sorting mechanisms and biological functions of raft domains.

https://dx.doi.org/10.1021/acs.analchem.0c00810
Anal. Chem. 2020, 92, 7232−7239

■ ASSOCIATED CONTENT

Supporting Information

The Supporting Information is available free of charge at https://pubs.acs.org/doi/10.1021/acs.analchem.0c00810.

Additional experimental section, scheme for reaction between Gal/GalNAc and FTZ (Figure S1), probe cytotoxicity assay (Figure S2), 7KC concentration optimization (Figure S3), CTxB-AF647 concentration optimization (Figure S4), and effect of GO on signal enhancement (Figure S5) (PDF)

■ AUTHOR INFORMATION

Corresponding Author

Lin Ding − *State Key Laboratory of Analytical Chemistry for Life Science, School of Chemistry and Chemical Engineering, Chemistry and Biomedicine Innovation Center (ChemBIC), Nanjing University, Nanjing 210023, People's Republic of China;* orcid.org/0000-0001-5381-3484; Phone: +86-25-89681927; Email: dinglin@nju.edu.cn

Authors

Jing Tao − *State Key Laboratory of Analytical Chemistry for Life Science, School of Chemistry and Chemical Engineering, Chemistry and Biomedicine Innovation Center (ChemBIC), Nanjing University, Nanjing 210023, People's Republic of China*

Xiaofei Yu − *State Key Laboratory of Analytical Chemistry for Life Science, School of Chemistry and Chemical Engineering, Chemistry and Biomedicine Innovation Center (ChemBIC), Nanjing University, Nanjing 210023, People's Republic of China*

Yuna Guo − *State Key Laboratory of Analytical Chemistry for Life Science, School of Chemistry and Chemical Engineering, Chemistry and Biomedicine Innovation Center (ChemBIC), Nanjing University, Nanjing 210023, People's Republic of China*

Guyu Wang − *State Key Laboratory of Analytical Chemistry for Life Science, School of Chemistry and Chemical Engineering, Chemistry and Biomedicine Innovation Center (ChemBIC), Nanjing University, Nanjing 210023, People's Republic of China*

Huangxian Ju − *State Key Laboratory of Analytical Chemistry for Life Science, School of Chemistry and Chemical Engineering, Chemistry and Biomedicine Innovation Center (ChemBIC), Nanjing University, Nanjing 210023, People's Republic of China;* orcid.org/0000-0002-6741-5302

Complete contact information is available at: https://pubs.acs.org/10.1021/acs.analchem.0c00810

Notes

The authors declare no competing financial interest.

■ ACKNOWLEDGMENTS

We gratefully acknowledge support from the National Natural Science Foundation of China (21974067, 21675082), the National Key Research and Development Program of China (2018YFC1004704), Fundamental Research Funds for the Central Universities (020514380184), and State Key Laboratory of Analytical Chemistry for Life Science (5431ZZXM1903, 5431ZZXM1801).

■ REFERENCES

(1) Sezgin, E.; Levental, I.; Mayor, S.; Eggeling, C. *Nat. Rev. Mol. Cell Biol.* **2017**, *18*, 361−374.
(2) Varma, R.; Mayor, S. *Nature* **1998**, *394*, 798−801.
(3) Anderson, R. G. W.; Jacobson, K. *Science* **2002**, *296*, 1821−1825.
(4) Simons, K.; Gerl, M. J. *Nat. Rev. Mol. Cell Biol.* **2010**, *11*, 688−699.
(5) Munro, S. *Cell* **2003**, *115*, 377−388.
(6) Allen, J. A.; Halverson-Tamboli, R. A.; Rasenick, M. M. *Nat. Rev. Neurosci.* **2007**, *8*, 128−140.
(7) Lingwood, D.; Simons, K. *Science* **2010**, *327*, 46−50.
(8) Cheng, X. L.; Smith, J. C. *Chem. Rev.* **2019**, *119*, 5849−5880.
(9) Ikonen, E. *Curr. Opin. Cell Biol.* **2001**, *13*, 470−477.
(10) Iwabuchi, K. *Front. Biosci., Landmark Ed.* **2015**, *20*, 325−334.
(11) Dick, R. A.; Goh, S. L.; Feigenson, G. W.; Vogt, V. M. *Proc. Natl. Acad. Sci. U. S. A.* **2012**, *109*, 18761−18766.
(12) Staubach, S.; Razawi, H.; Hanisch, F. G. *Proteomics* **2009**, *9*, 2820−2835.
(13) Raghu, H.; Sodadasu, P. K.; Malla, R. R.; Gondi, C. S.; Estes, N.; Rao, J. S. *BMC Cancer* **2010**, *10*, 647−664.
(14) Larsen, J. B.; Jensen, M. B.; Bhatia, V. K.; Pedersen, S. L.; Bjørnholm, T.; Iversen, L.; Uline, M.; Szleifer, I.; Jensen, K. J.; Hatzakis, N. S.; Stamou, D. *Nat. Chem. Biol.* **2015**, *11*, 192−194.
(15) Hanada, K.; Nishijima, M.; Akamatsu, Y.; Pagano, R. E. *J. Biol. Chem.* **1995**, *270*, 6254−6260.
(16) Foster, L. J.; de Hoog, C. L.; Mann, M. *Proc. Natl. Acad. Sci. U. S. A.* **2003**, *100*, 5813−5818.
(17) Ando, J.; Kinoshita, M.; Cui, J.; Yamakoshi, H.; Dodo, K.; Fujita, K.; Murata, M.; Sodeoka, M. *Proc. Natl. Acad. Sci. U. S. A.* **2015**, *112*, 4558−4563.
(18) Prior, I. A.; Muncke, C.; Parton, R. G.; Hancock, J. F. *J. Cell Biol.* **2003**, *160*, 165−170.
(19) Klymchenko, A. S.; Kreder, R. *Chem. Biol.* **2014**, *21*, 97−113.
(20) Blank, N.; Schiller, M.; Krienke, S.; Wabnitz, G.; Ho, A. D.; Lorenz, H. M. *Immunol. Cell Biol.* **2007**, *85*, 378−382.
(21) Asanov, A.; Zepeda, A.; Vaca, L. *Biochim. Biophys. Acta, Mol. Cell Biol. Lipids* **2010**, *1801*, 147−155.
(22) Komura, N.; Suzuki, K. G. N.; Ando, H.; Konishi, M.; Koikeda, M.; Imamura, A.; Chadda, R.; Fujiwara, T. K.; Tsuboi, H.; Sheng, R.; Cho, W.; Furukawa, K.; Furukawa, K.; Yamauchi, Y.; Ishida, H.; Kusumi, A.; Kiso, M. *Nat. Chem. Biol.* **2016**, *12*, 402−410.
(23) Jiang, Y.-W.; Guo, H.-Y.; Chen, Z.; Yu, Z.-W.; Wang, Z. F.; Wu, F.-G. *Langmuir* **2016**, *32*, 6739−6745.
(24) Dent, M. R.; López-Duarte, I.; Dickson, C. J.; Chairatana, P.; Anderson, H. L.; Gould, I. R.; Wylie, D.; Vyšniauskas, A.; Brooks, N. J.; Kuimova, M. K. *Chem. Commun.* **2016**, *52*, 13269−13272.
(25) Tian, M. G.; Liu, Y.; Sun, Y. M.; Zhang, R. Y.; Feng, R. Q.; Zhang, G.; Guo, L. F.; Li, X. C.; Yu, X. Q.; Sun, J. Z.; He, X. Q. *Biomaterials* **2017**, *120*, 46−56.
(26) Shao, B. J.; Yago, T.; Setiadi, H.; Wang, Y.; Mehta-D'souza, P.; Fu, J. X.; Crocker, P. R.; Rodgers, W.; Xia, L. J.; McEver, R. P. *Proc. Natl. Acad. Sci. U. S. A.* **2015**, *112*, 8661−8666.
(27) Gaudin, R.; Barteneva, N. S. *Nat. Commun.* **2015**, *6*, 6022.
(28) Beutel, O.; Nikolaus, J.; Birkholz, O.; You, C. J.; Schmidt, T.; Herrmann, A.; Piehler, J. *Angew. Chem.* **2014**, *126*, 1335−1339.
(29) Ohtsubo, K.; Marth, J. D. *Cell* **2006**, *126*, 855−867.
(30) Hamilton, G. A.; Adolf, P. K.; De Jersey, J.; DuBois, G. C.; Dyrkacz, G. R.; Libby, R. D. *J. Am. Chem. Soc.* **1978**, *100*, 1899−1912.
(31) Whittaker, J. W. *Arch. Biochem. Biophys.* **2005**, *433*, 227−239.
(32) Hui, J. J.; Bao, L.; Li, S. Q.; Zhang, Y.; Feng, Y. M.; Ding, L.; Ju, H. X. *Angew. Chem., Int. Ed.* **2017**, *56*, 8139−8143.
(33) Zhang, P. W.; Li, Y. R.; Yu, X. F.; Ju, H. X.; Ding, L. *Chem. - Eur. J.* **2019**, *25*, 10505−10510.
(34) Pinho, S. S.; Reis, C. A. *Nat. Rev. Cancer* **2015**, *15*, 540−555.
(35) Dreaden, E. C.; Alkilany, A. M.; Huang, X. H.; Murphy, C. J.; Elsayed, M. A. *Chem. Soc. Rev.* **2012**, *41*, 2740−2779.
(36) Grabar, K. C.; Freeman, R. G.; Hommer, M. B.; Natan, M. J. *Anal. Chem.* **1995**, *67*, 735−743.

(37) Park, J.; Shin, J. H.; Park, J.-K. *Anal. Chem.* **2016**, *88*, 3781−3788.
(38) Aioub, M.; El-Sayed, M. A. *J. Am. Chem. Soc.* **2016**, *138*, 1258−1264.
(39) Setiadi, H.; McEver, R. P. *Blood* **2008**, *111*, 1989−1998.
(40) Dalton, G.; An, S.-W.; Al-Juboori, S. I.; Nischan, N.; Yoon, J.; Dobrinskikh, E.; Hilgemann, D. W.; Xie, J.; Luby-Phelps, K.; Kohler, J. J.; Birnbaumer, L.; Huang, C. L. *Proc. Natl. Acad. Sci. U. S. A.* **2017**, *114*, 752−757.
(41) Macdonald, J. L.; Pike, L. J. *J. Lipid Res.* **2005**, *46*, 1061−1067.
(42) Owen, D. M.; Williamson, D. J.; Magenau, A.; Gaus, K. *Nat. Commun.* **2012**, *3*, 1256.
(43) Paek, J.; Kalocsay, M.; Staus, D. P.; Wingler, L.; Pascolutti, R.; Paulo, J. A.; Gygi, S. P.; Kruse, A. C. *Cell* **2017**, *169*, 338−349.
(44) Nichols, B. J.; Kenworthy, A. K.; Polishchuk, R. S.; Lodge, R.; Roberts, T. H.; Hirschberg, K.; Phair, R. D.; Lippincott-Schwartz, J. *J. Cell Biol.* **2001**, *153*, 529−542.
(45) Lobingier, B. T.; Hüttenhain, R.; Eichel, K.; Miller, K. B.; Ting, A. Y.; von Zastrow, M.; Krogan, N. J. *Cell* **2017**, *169*, 350−360.

https://dx.doi.org/10.1021/acs.analchem.0c00810
Anal. Chem. 2020, 92, 7232−7239